

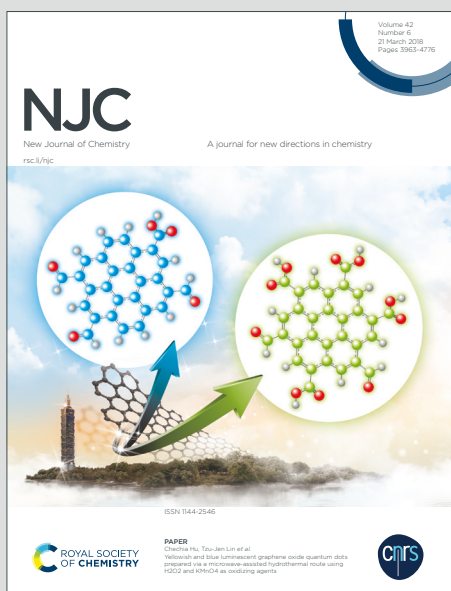
NJC

New Journal of Chemistry

Accepted Manuscript

A journal for new directions in chemistry

This article can be cited before page numbers have been issued, to do this please use: Z. Zhou, X. Li, Y. Wang, Y. Luan, X. Li and X. Du, *New J. Chem.*, 2020, DOI: 10.1039/D0NJ02672G.



This is an Accepted Manuscript, which has been through the Royal Society of Chemistry peer review process and has been accepted for publication.

Accepted Manuscripts are published online shortly after acceptance, before technical editing, formatting and proof reading. Using this free service, authors can make their results available to the community, in citable form, before we publish the edited article. We will replace this Accepted Manuscript with the edited and formatted Advance Article as soon as it is available.

You can find more information about Accepted Manuscripts in the [Information for Authors](#).

Please note that technical editing may introduce minor changes to the text and/or graphics, which may alter content. The journal's standard [Terms & Conditions](#) and the [Ethical guidelines](#) still apply. In no event shall the Royal Society of Chemistry be held responsible for any errors or omissions in this Accepted Manuscript or any consequences arising from the use of any information it contains.

ARTICLE

Growth of Cu-BTC MOFs on dendrimer-like porous silica nanospheres for catalytic aerobic epoxidation of olefins

Zihao Zhou,^a Xiujuan Li,^a Yulin Wang,^a Yi Luan,^{*a} Xiaoyu Li ^{*b} and Xin Du ^{*a}Received 00th January 20xx,
Accepted 00th January 20xx

DOI: 10.1039/x0xx00000x

The composition of Metal-organic frameworks (MOFs) and porous carriers can be utilized for a variety of material applications. In this study, DPSNs@Cu-BTC nanocomposites is achieved utilizing Dendrimer-like Porous Silica Nanoparticles (DPSNs) as the support through a template-mediated self-assembly mechanism. The fabrication process initiated from the controllable growth of Cu₂O nanoparticles (NPs) in the center-radial porous channels of DPSNs, which forms DPSNs@Cu₂O nanocomposites. Under the protection of DPSNs, the loaded Cu₂O NPs gradually dissolved in the weak acid solution, thus providing copper ions to guide the formation and growth of Cu-BTC nanocrystals. Moreover, the Cu-BTC NPs were restricted in the center-radial porous channels of the DPSNs, thus resulting in small sizes and a uniform distribution. The formation of the DPSNs@Cu-BTC nanocomposites with adjustable amounts of Cu-BTC mainly depended on the amounts of Cu₂O NPs loaded and the amount of organic ligands added. Furthermore, the nanocomposite exhibited high catalytic performance and good recyclability taking advantage of the uniform loading of small-sized Cu-BTC NPs in the accessible center-radial porous channels of the DPSNs. This new design of DPSNs@Cu-BTC provided a new approach for the synthesis of various MOF-based nanocomposites with improved performance.

1. Introduction

Metal-organic frameworks (MOFs) are a class of porous materials consisting of multi-topic organic ligands and metal ions.¹⁻³ As analogues of zeolites, MOFs with high specific surface area and extremely regular channels can be applied to many fields, such as gas storage and separation, catalysis, sensing, theranostics, etc.⁴⁻⁷ Although MOFs as heterogeneous catalysts have produced a few ground-breaking results, greater progress has been hampered due to the lower chemical and mechanical stability of MOFs compared to zeolites.⁸ The immobilization of MOFs onto/into supports (MOFs-based nanocomposites) may be one way to overcome this issue.

As an intensively studied MOF, [Cu₃(BTC)₂] (Cu-BTC, BTC = 1,3,5-benzenetricarboxylate) (named also HKUST-1 or MOF-199) has dimeric cupric tricarboxylate units with a short Cu-Cu internuclear separation, which induces attractive catalytic activities in various catalysts, such as Diels-Alder reactions,⁹ esterification¹⁰ and Friedländer reaction.¹¹ Therefore, the design and controllable fabrication of Cu-BTC-based composite nanocatalysts have attracted much attention in recent years.¹²⁻¹⁵ For example, Sachse et al. reported a macro-/mesoporous silica monolith-supported Cu-BTC catalyst.¹² Zhang's group fabricated a Cu-BTC-SiO₂ monolith composite for the selective

oxidation of alkylbenzenes.¹³ Martyanov's laboratory prepared HKUST-1@silica aerogel composite pellets (HKUST-1@SiO₂) by the coupled sol-gel and water-in-oil emulsion method.¹⁴ Sun's team fabricated MOF-5 (HKUST-1 or ZIF-8) inside two-dimensional hexagonal pores of SBA-15 using a double-solvent strategy with significantly enhanced hydrostability and catalytic activity.¹⁵ Among various porous materials, dendrimer-like porous silica nanospheres (DPSNs) may have great potential as a carrier to support and protect Cu-BTC NPs due to center-radial large pores and interconnected wrinkles on the particle surface.¹⁶⁻²⁰ Some Cu-BTC/SiO₂ composite materials have been reported.²¹⁻²⁴ Compared with conventional ordered mesoporous silicas, DPSNs have unique three-dimensional superstructures with accessible pore surfaces and high pore volumes. However, there is no report about the composite of DPSNs and Cu-BTC. There are two main possible reasons for their combination having been restricted up to now. First, the particle size of DPSNs is usually less than 500 nm and the surface pore size less than 100 nm, while the size of Cu-BTC NPs is generally more than 500 nm. This mismatch makes it difficult to grow Cu-BTC NPs in the center-radial porous channels of DPSNs or even to form a Cu-BTC coating on the surface of DPSNs. Secondly, DPSNs without surface functionalization lack the functional groups to anchor copper ions or organic ligands, and conventional physical adsorption is also not sufficient. In addition, although surface functionalization can anchor some copper ions or organic ligands, the Cu-BTC may be separated from the surface or pore of the DPSNs due to its large size. Therefore, it is necessary to develop new strategies to achieve the controllable loading of Cu-BTC NPs in the center-radial porous channels of DPSNs.

^a School of Materials Science and Engineering, University of Science and Technology Beijing, 30 Xueyuan Road, Haidian District, Beijing 100083, P. R. China. E-mail: yiluan@ustb.edu.cn, duxin@ustb.edu.cn

^b National Engineering Laboratory for Hydrometallurgical Cleaner Production Technology, Key Laboratory of Green Process and Engineering, Institute of Process Engineering, Chinese Academic of Sciences, Beijing 100190, China. E-mail: lixy@ipe.ac.cn

In the present study, DPSNs@Cu–BTC nanocomposites were prepared by first growing Cu₂O NPs in the center-radial porous channels of DPSNs and then creating a reaction between DPSNs@Cu₂O and 1,3,5-benzenetricarboxylic acid (H₃BTC) by dissolution in acid, oxidation and self-assembly. Additionally, Cu₂O was chosen instead of CuO because the chemical stability of Cu₂O is relatively poor and it can be dissolved by the acidity of the H₃BTC ligand without producing residual Cu₂O. Introducing Cu₂O NPs into DPSNs pores by indirect fabrication not only solves the problem that Cu–BTC cannot be directly grown in the pores of DPSNs, but also makes full use of the effect of confining the center-radial porous channels to reduce the sizes of the Cu–BTC NPs thus formed. It is expected that the homogeneous distribution of small-sized Cu–BTC in the pores of the DPSNs can construct DPSNs@Cu–BTC nanocomposites with good catalytic performance and cycle stability in the epoxidation of olefins.

2. Experimental section

2.1 Materials

Tetraethyl orthosilicate (TEOS, 99%), cetyltrimethylammonium tosylate (CTA Tos, 98%), triethanolamine (TEA, 99%), 3-aminopropyltriethoxysilane (APTES, 98%), L-Ascorbic acid (Sigma-Aldrich, 99%), benzyl alcohol (Aldrich, 99%), and *cis*-Cyclooctene (C₈H₁₄, 99%) were purchased from Sigma Aldrich. Aqueous ammonia (NH₃·H₂O, 25%), concentrated hydrochloric acid (HCl, 37%), toluene (99%), absolute ethanol (99%), copper nitrate trihydrate (Cu(NO₃)₂·3H₂O, 99%), poly-(vinylpyrrolidone) (PVP, K-30), and acetonitrile (CH₃CN, 99%) were purchased from Beihua Fine Chemicals. 1,3,5-benzenetricarboxylic acid (H₃BTC, 95%) was purchased from Alfa Aesar. Ultrapure water with a resistivity higher than 18.2 MΩ·cm, which was obtained from a three-stage Millipore Mill-Q Plus 185 purification system (Academic), was used in all experiments. All reagents with analytical grade were used as received.

2.2 Characterization

For transmission electron microscopy (TEM) observations, powder samples were added on carbon-coated copper grids and observed on a JEOL JEM-2100F transmission electron microscope equipped with an energy dispersive X-ray spectrometer (EDX) at an acceleration voltage of 200 kV. The phase composition of the samples was analyzed by powder X-ray diffraction (XRD, M21X) with Cu K α radiation (40 kV, 150 mA, $\lambda=1.5406$ Å). The copper content of the samples was measured with inductively coupled plasma-atomic emission spectrometry (ICP-AES). Chemical compositions were obtained using X-ray photoelectron spectroscopy (XPS, Shimadzu ESCA-3200). Fourier transform infrared spectra (FTIR) were obtained using a Nicolet 6700 Fourier spectrometer. The specific surface areas of the catalysts were calculated by the BET (Brunauer-Emmett-Teller) method, and the pore-size distributions of the catalysts were derived from the adsorption branches of isotherms by Barrett-Joyner-Halenda (BJH) method.

2.3 Synthesis of the DPSNs

Monodispersed DPSNs were prepared by using CTA-Tos as a surfactant, [BMIM] OTF as a co-surfactant, TEA as a mineralizing agent, water as a solvent and TEOS as a silica precursor. A typical synthesis of DPSNs with a size of ca. 245±26 nm was performed as follows: a mixture of CTA-Tos (0.96 g), [BMIM] OTF (0.30 g), TEA (0.105 g) and water (50 mL) was stirred at 80 °C for 1 h, and then TEOS (7.8 mL) was quickly added into the surfactant solution. The mixture was stirred at a speed of 1000 rpm at 80 °C for another 2 h. The DPSNs thus formed were filtered, washed, and dried in an oven at 60 °C. The CTA-Tos was removed from particles by template extraction. The as-prepared DPSNs (1.0 g) were added into ethanolic HCl (concentrated HCl (15 mL) in ethanol (100 mL), and sonicated for 2 h. The suspension was stirred at 70 °C for 24 h. The extraction procedure was repeated three times to efficiently remove the surfactant. Finally, the precipitates were centrifuged, washed with ethanol, and dried in air at 60 °C.

2.4 Synthesis of the DPSNs@Cu₂O

DPSNs@Cu₂O nanocomposites were synthesized following the reported procedure with some modifications.²⁵ In a typical synthesis, PVP (1.0 g) was fully dissolved in Cu(NO₃)₂ aqueous solution (0.01 M, 50 mL) under vigorous magnetic stirring. DPSNs (50 mg) and L-Ascorbic acid (70 mg) were mixed in water (2.0 mL), which was then quickly injected into the Cu(NO₃)₂ aqueous solution, followed by the immediate introduction of NH₃·H₂O aqueous solution (60 μ L). Typically, the color changed to dark red-yellow within 5 s, indicating the formation of Cu₂O. The reaction mixture was kept stirring for 2 min, and the product was collected by centrifugation at 8000 rpm for 10 min. Subsequently, the NPs were washed with ethanol and deionized water (volume ratio 1:1) three times to remove excess PVP, and were redispersed in benzyl alcohol (BnOH, 2.5 mL), and stored in a refrigerator at 4.0 °C. DPSNs@Cu₂O with theoretical load percentages of 10, 20 and 30 wt.% were fabricated by adjusting the amount of L-Ascorbic acid from 17.5 mg to 70 mg, the volume of Cu(NO₃)₂ solution (12.5, 25, 50 mL) and different amounts of NH₃·H₂O (15, 30, 60 μ L), respectively (Table S1).

2.5 Synthesis of the DPSNs@Cu–BTC

DPSNs@Cu–BTC nanocomposites were synthesized by increasing the dosage and providing additional oxygen, following the partial procedure of Au NPs@Cu–BTC.²⁶ H₃BTC (0.275 mmol) was added into a mixture of BnOH (7.5 mL) and ethanol (0.5 mL), and then sonicated for 30 min to achieve a homogeneous solution. Subsequently, 2.5 mL of DPSNs@Cu₂O NPs in BnOH was added, followed immediately by an O₂ balloon, and then reacted at 80 °C overnight unless otherwise noted. The product was collected by centrifuging at 5000 rpm for 5 min, washed with methanol several times, and finally dried at room temperature. In addition, the loading capacity of Cu–BTC on the DPSNs was controlled by adjusting different Cu₂O amounts (Table S2). The percentages of copper species being introduced into the DPSNs were determined to be 1.4, 4.0 and 9.2 wt.% for

DPSNs@Cu-BTC-1, DPSNs@Cu-BTC-2 and DPSNs@Cu-BTC-3 via ICP-AES.

2.6 Synthesis of the DPSNs@Cu-BTC

The catalytic performance of the catalysts was investigated by the aerobic epoxidation of olefins. The olefin substrate (1.0 mmol), pivalaldehyde (2.0 mmol), and the DPSNs@Cu-BTC catalyst (2.0 mol % based on copper content) were dissolved in acetonitrile (5.0 mL). The mixture was then stirred at 40 °C for 6 h under oxygen atmosphere. After the reaction, the catalyst was separated by centrifugation. The reaction liquid solution was analyzed by GC-MS using nitrobenzene as the internal standard.

2.7 Synthesis of the DPSNs@Cu-BTC

The recyclability of the catalyst was examined by using the recovered DPSNs@Cu-BTC catalyst in the aerobic epoxidation of cyclooctene under optimal reaction conditions. The catalyst was separated, washed with ethanol three times, dried and reused for the next cycle reaction.

3. Results and discussion

3.1 Structure and composition of the DPSNs@Cu-BTC

DPSNs@Cu-BTC nanocomposites were prepared by two steps, as shown in the schematic illustration of the synthesis mechanism (Fig. 1). First, Cu₂O NPs were deposited into the center-radial pore channels of DPSNs to form DPSNs@Cu₂O composites by using copper nitrate as copper source and ascorbic acid as reducing agent via a simple chemical deposition method. Second, DPSNs@Cu₂O composites was used as the precursor to prepare DPSNs@Cu-BTC based on the acidic dissolution and O₂ oxidation of Cu₂O NPs and the self-assembly between H₃BTC and Cu²⁺ ions. The chemical reaction equation is $2\text{Cu}_2\text{O} + \text{O}_2 + 8\text{H}^+ \rightarrow 4\text{Cu}^{2+} + 4\text{H}_2\text{O}$. In the synthesis process, the unique radial pore structure of DPSNs had three main advantages: (1) The dispersion of small Cu₂O NPs was improved by being loaded in the center-radial pore channels, thus avoiding the formation of large-size Cu₂O NPs and the problem of residual Cu₂O caused by inadequate reaction during the Cu-BTC formation process. (2) The growth of Cu-BTC was limited, resulting in the formation of small-size Cu-BTC with high catalytic activity. (3) The chemical stability of Cu-BTC was improved through the support and protection of the DPSNs.

We conducted TEM measurement to characterize the surface morphology of DPSNs@Cu₂O and DPSNs@Cu-BTC composites, as shown in Fig. 2. The DPSNs have a mean particle size of ca. 245 ± 25 nm, which have a central radial channel and shows a dendritic porous structure (Fig. S1). For DPSNs@Cu₂O composites, Cu₂O NPs of small sizes are distributed in the central radial pore channels of the DPSNs. As greater amounts of Cu₂O NPs are loaded, their sizes grow from ~10 nm to ~30 nm, and the amount of Cu₂O NPs also increases (Fig. 2 a1, b1, c1). In the DPSNs@Cu-BTC composites, the formed Cu-BTC NPs have a small size of 40±25 nm, and exhibit a homogeneous distribution without agglomeration (Fig. 2 a2, b2, c2). As more and more Cu-BTC is loaded, the size of the Cu-BTC NPs shows no obvious change, but their quantity increases. This may result from the fact that Cu-BTC grows from the inside of DPSNs channels to the outside and is limited by the channels. In addition, the dispersion of the DPSNs@Cu-BTC is inversely proportional to the amounts of Cu-BTC loaded (Fig. 2 a3, b3, c3). This is because the Cu-BTC grown outside the pore channel can agglomerate with the Cu-BTC on the surface of other DPSNs. When the amount loaded is particularly large (about 70 wt.% of Cu-BTC), large-sized Cu-BTC NPs with an octahedral structure form on the surface of the DPSNs. In addition to the developed synthesis method in this work, we also tried other methods such as hydrothermal synthesis,²⁷ ultrasonic synthesis,²⁸ ethanol reflux²⁹ and layer by layer coating.³⁰ TEM images of the composites prepared by these methods are shown in Fig. S2. The results show that none of these composites can achieve the growth of Cu-BTC in the center-radial pores of the DPSNs. This can be attributed to the growth rate of the Cu-BTC prepared by these methods being too fast, and the sizes of the formed Cu-BTC NPs being larger than the pore sizes of the DPSNs. Moreover, the small size of the Cu-BTC makes it agglomerate easily. Therefore, the key to the successful preparation of DPSNs@Cu-BTC nanocomposites is to reduce the growth rate and size. In this work the growth rate was reduced by dissolving Cu₂O to release copper ions, and the size was reduced by confined growth in the pore channels of the DPSNs. By adjusting the loading capacity of the Cu₂O, DPSNs@Cu-BTC nanocomposites with different Cu-BTC loading amounts were obtained.

The powder XRD patterns of DPSNs@Cu₂O shown in Fig. S3 are consistent with those of Cu₂O,^{25,31} and reveal the successful synthesis of Cu₂O. As shown in powder PXRD patterns (Fig. 3),

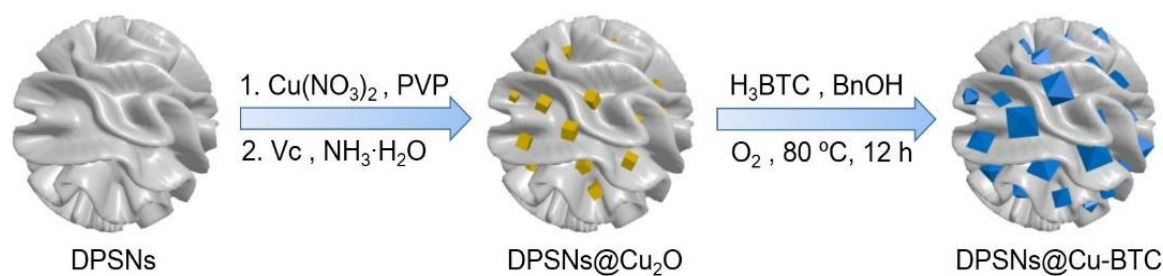
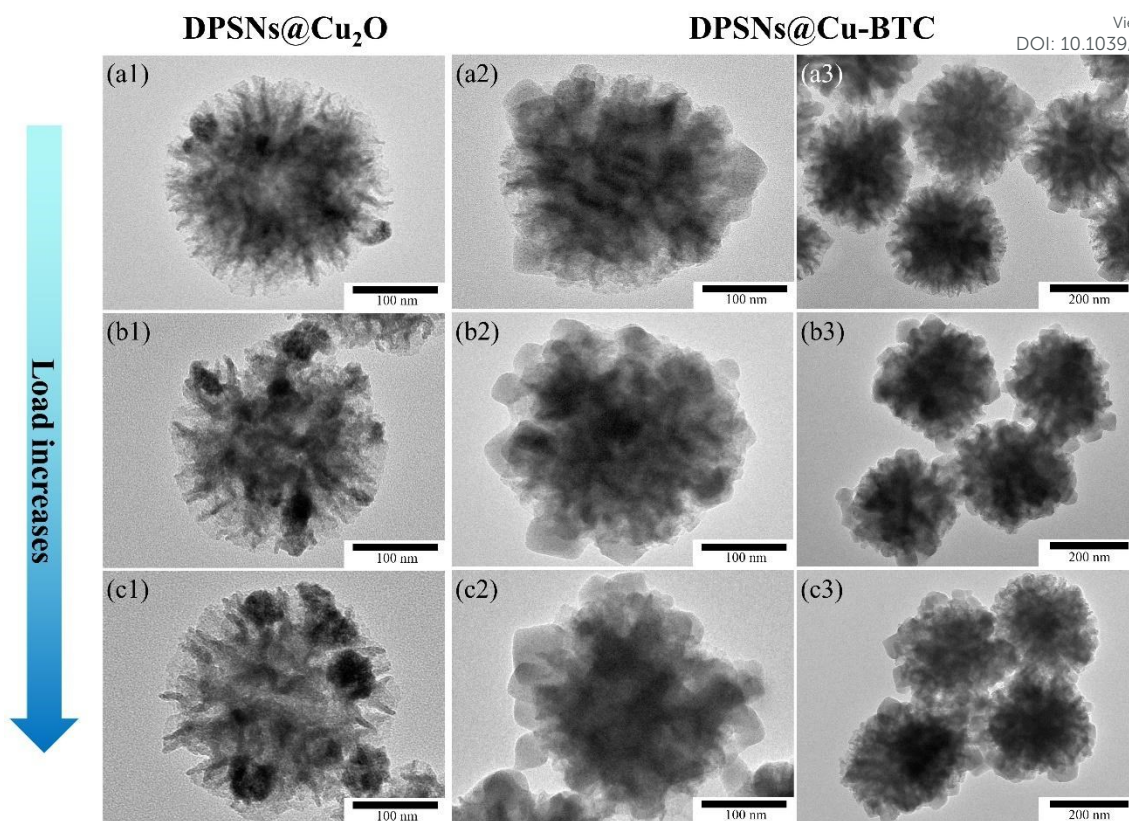


Fig. 1 Schematic illustration of the formation mechanism of DPSNs@Cu-BTC composite.



View Article Online
DOI: 10.1039/D0NJ02672G

Fig. 2 TEM images of DPSNs@Cu₂O and DPSNs@Cu-BTC: (a1) DPSNs@Cu₂O-1, (b1) DPSNs@Cu₂O-2, (c1) DPSNs@Cu₂O-3, (a2 and a3): DPSNs@Cu-BTC-1, (b2 and b3): DPSNs@Cu-BTC-2, (c2 and c3): DPSNs@Cu-BTC-3.

all the diffraction peaks of DPSNs@Cu-BTC composites correspond well with those of Cu-BTC.^{27,32} This illustrates that the DPSNs did not change the structure of the Cu-BTC, and that their structure remained stable during the growth of the Cu-BTC. Interestingly, as shown in Fig. S4, the Cu-BTC prepared from Cu₂O NPs still has the characteristic peak of Cu₂O. And the TEM images also show significant residual Cu₂O (Fig. S5). This indicates that the Cu-BTC NPs made from Cu₂O NPs contain residual Cu₂O which has not been completely reacted.

Interestingly, there is basically no residual Cu₂O in the DPSNs@Cu-BTC made from DPSNs@Cu₂O. Even when the amounts of Cu₂O loaded increase to more than 60 wt.%, there is still no characteristic peak of Cu₂O in the DPSNs@Cu-BTC prepared by DPSNs@Cu₂O (Fig. S6). Although the TEM images (Fig. S7) show that the size of the Cu-BTC NPs is much larger than the pore size of the DPSNs, there is still no residual Cu₂O, which proves that the DPSNs play an important role in dispersing the Cu₂O NPs inside the pore channels and avoiding incomplete reaction caused by the agglomeration of the Cu₂O.

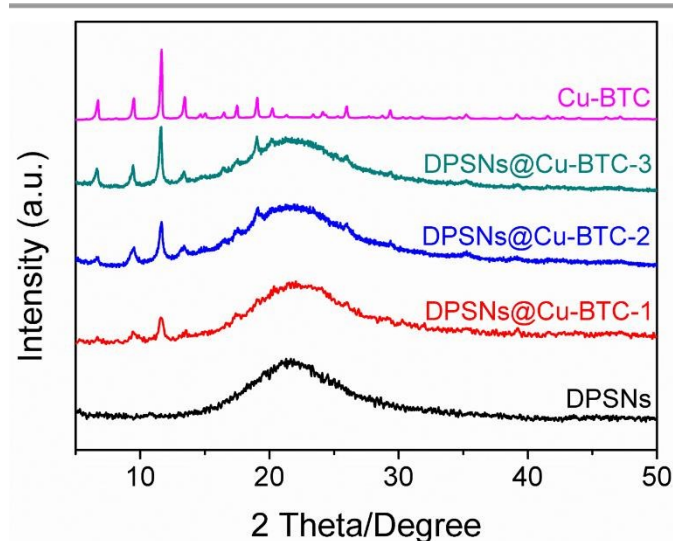


Fig. 3 X-ray diffraction patterns of DPSNs@Cu-BTC, DPSNs and Cu-BTC.

In order to further study the distribution of Cu-BTC NPs in DPSNs@Cu-BTC heterostructure, EDX imaging and spectroscopic measurement were performed. Cu-BTC basically contains only copper, carbon and oxygen elements, while DPSNs only contain silicon and oxygen elements. Therefore, as shown in Fig. 4, it is obvious from the distribution of the copper and carbon elements that small-sized Cu-BTC distributes evenly outside DPSNs. From silicon element, DPSNs still have dendrimer-like structure, which proves that Cu-BTC NPs do not completely encapsulate all the DPSNs, but grow outward from the inside of the pores. Furthermore, the morphology of the DPSNs is retained under the current synthetic method.

The TGA curve of the Cu-BTC prepared from Cu₂O was shown in Fig. S8. The weight reduction at 40-285 °C is caused by the volatilization of water, ethanol and other solvent molecules in the Cu-BTC (about 7.0 wt.%). At 285-386 °C, 1,3,5-benzenetricarboxylic acid, an organic ligand, decomposes violently along with a sharp decrease in weight (about 36 wt.%),

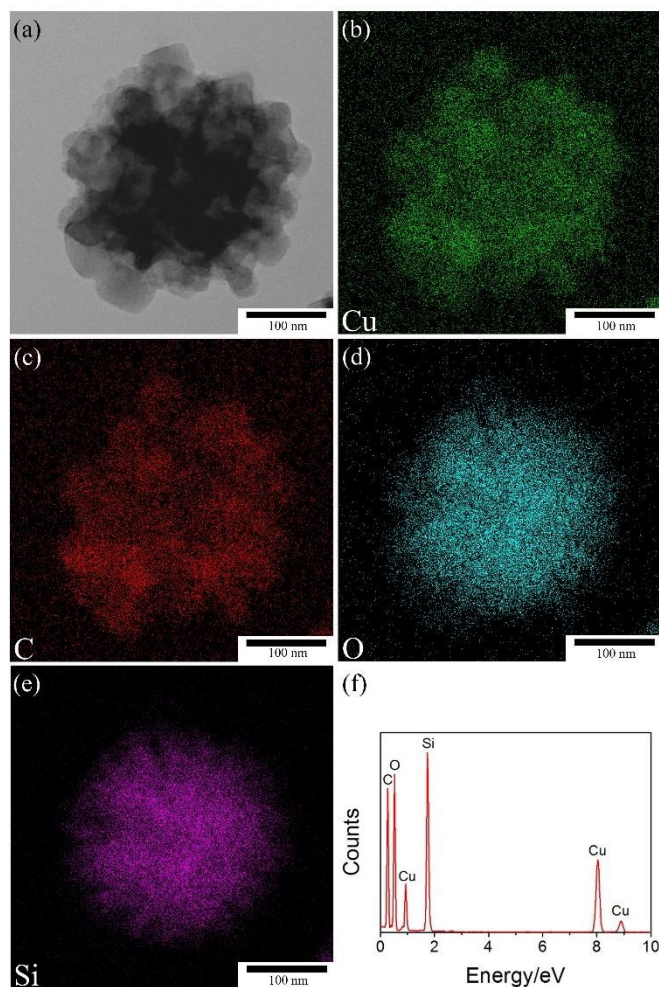


Fig. 4 (a) TEM images of DPSNs@Cu-BTC-2, (b-e) EDX elemental maps of Cu, C, O, Si in DPSNs@Cu-BTC-2, (f) EDX spectrum of DPSNs@Cu-BTC-2.

and Cu-BTC is degraded into CuO. After 386 °C, the loss of weight tended to be slow. The TGA curves of the three DPSNs@Cu-BTC nanocomposites are similar. As shown in Fig. 5, the weights of the composites decrease slightly in the temperature range of 40–285 °C, due to the evaporation of the water and the decomposition of the residual species. As the temperature increases, the TGA curves are markedly different as a result of the different amounts of Cu-BTC loaded in each composite. And the final residual mass is 80, 75 and 68 wt.%, respectively, for DPSNs@Cu-BTC-1, DPSNs@Cu-BTC-2 and DPSNs@Cu-BTC-3. This proves that the amounts of Cu-BTC loaded can be precisely controlled by adjusting the amounts of Cu₂O loaded.

In order to study the oxidation state of copper ion in the composites, XPS measurement was carried out for the DPSNs@Cu-BTC-2, which was selected due to its having the best catalytic performance. Specifically, all the elements in the DPSNs@Cu-BTC-2 are Si, C, O and Cu, which is consistent with the element types of the EDX spectrum (Fig. 6a). There are three typical shakeup satellite peaks (S1, S2 and S3) in the Cu 2p regions, indicating that they are Cu²⁺. The strong Cu 2p_{3/2} and Cu 2p_{1/2} peaks fitted by Cu²⁺ are 934.4 and 954.3 eV,

respectively. For Cu⁺, the very weak Cu 2p_{3/2} and Cu 2p_{1/2} peaks are located at 932.4 and 952.3 eV, respectively, indicating the content is very low (Fig. 6b).

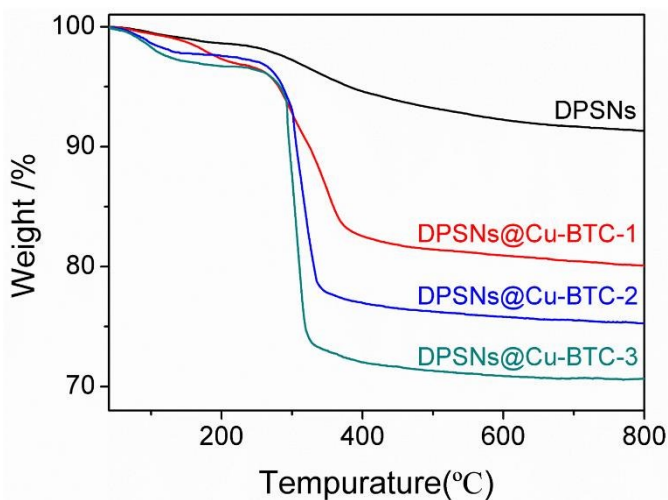


Fig. 5 TGA diagrams of DPSNs@Cu-BTC and DPSNs.

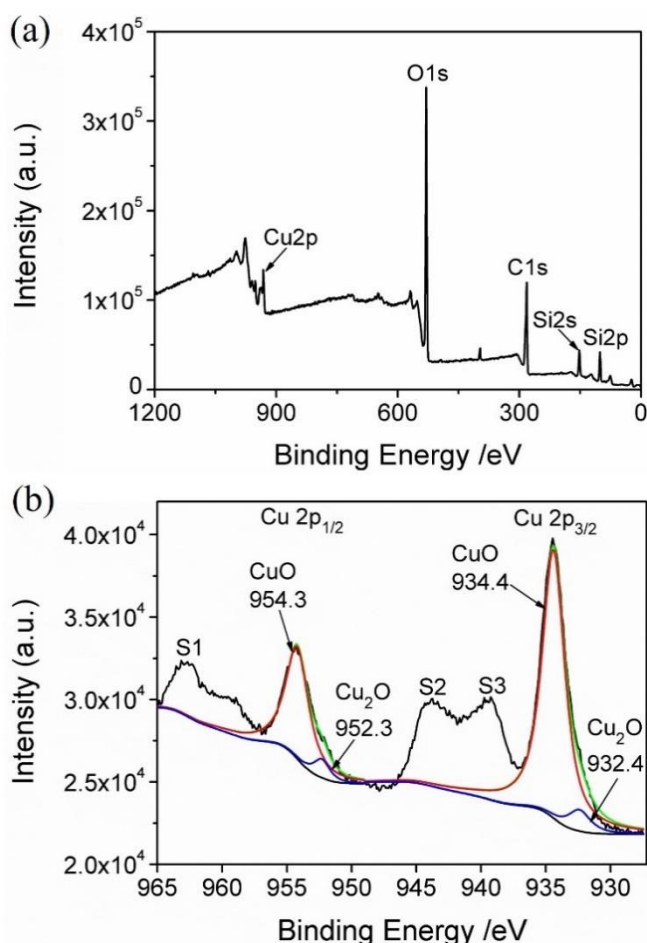


Fig. 6 XPS Analysis of DPSNs@Cu-BTC-2: (a) all elements, (b) Cu 2p Regions.

Fig. 7 represents the porosity properties of the DPSNs@Cu-BTC-2 examined by the N₂ adsorption-desorption method. As showed Fig. 7a, the isotherm mode of DPSNs@Cu-BTC-2 was

type I and similar with Cu-BTC (Fig. 7b), indicating the microporous properties. The BET surface area of the DPSNs@Cu-BTC-2 ($\sim 728 \text{ m}^2/\text{g}$) was between DPSNs ($\sim 282 \text{ m}^2/\text{g}$) and Cu-BTC ($\sim 1482 \text{ m}^2/\text{g}$). The new pore structure was formed due to the center-radial porous channels of DPSNs and the inevitable defects at the intersection of adjacent Cu-BTC or Cu-BTC and DPSNs.

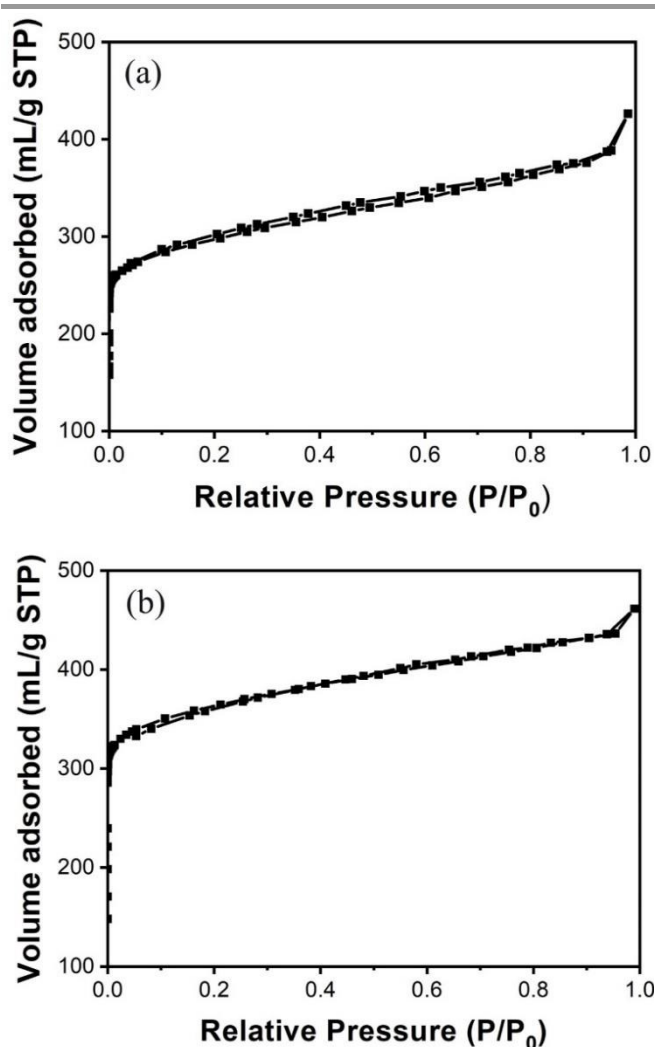


Fig. 7 N_2 adsorption-desorption isotherms of (a) DPSNs@Cu-BTC-2, (b) Cu-BTC.

3.2 Aerobic epoxidation of olefins

Taking the epoxidation of cyclooctene as the target reaction, we optimized our catalyst and reaction solvent as shown in Table 1. Under standard experimental conditions, the control reactions in the absence of catalyst give no reaction product in 4 h under an oxygen atmosphere (Entries 1-2). All the DPSNs@Cu-BTC nanocomposites loaded with different amounts of Cu-BTC are highly efficient in facilitating reactions, which are 92%, 99% and 99% of conversion, respectively (Entries 3-5). Interestingly, the DPSNs@Cu-BTC performs better than the Cu-BTC prepared by hydrothermal method (Entry 6). The reason for this may be that the smaller size Cu-BTC of the DPSNs@Cu-BTC is evenly

distributed in the center-radial pore channels, and more active sites are exposed to contact with the substrate. Furthermore, the conversions observed using the same amount of copper salts as epoxidation catalysts are 28% and 67%, respectively (Entries 7-8). A series of solvent screenings was carried out to determine the optimal solvent for the epoxidation of olefins. Acetonitrile is found to be the best solvent using other organic reagents as reaction solvent (Entries 9-12).

Table 1 Catalyst optimization experiments for the epoxidation of cyclooctene^a.

| Entry | Catalyst | Solvent | Con. (%) ^b | Sel. (%) ^b |
|-------|--|--------------|-----------------------|-----------------------|
| 1 | - | Acetonitrile | 9 | >99 |
| 2 | DPSNs | Acetonitrile | 8 | >99 |
| 3 | DPSNs@Cu-BTC-1 | Acetonitrile | 92 | >99 |
| 4 | DPSNs@Cu-BTC-2 | Acetonitrile | >99 | >99 |
| 5 | DPSNs@Cu-BTC-3 | Acetonitrile | >99 | >99 |
| 6 | Cu-BTC | Acetonitrile | 87 | >99 |
| 7 | $\text{CuCl}_2 \cdot 2\text{H}_2\text{O}$ | Acetonitrile | 28 | >99 |
| 8 | $\text{Cu}(\text{NO}_3)_2 \cdot 3\text{H}_2\text{O}$ | Acetonitrile | 67 | >99 |
| 9 | DPSNs@Cu-BTC-2 | Ethanol | <5 | >99 |
| 10 | DPSNs@Cu-BTC-2 | Acetone | 46 | >99 |
| 11 | DPSNs@Cu-BTC-2 | Toluene | 12 | >99 |
| 12 | DPSNs@Cu-BTC-2 | THF | <5 | >99 |

[a] Reaction conditions: 1.0 mmol cyclooctene, 2.0 mol% catalyst based on copper, trimethylacetaldehyde (2.0 mmol), 5.0 mL solvent, 1 atm O_2 , 40 °C, 4 h. [b] Nitrobenzene was used as internal standard and determined by GC-MS.

After obtaining the optimal reaction conditions, a collection of olefins was tested in order to prove the applicability of DPSNs@Cu-BTC-2 as catalyst for aerobic epoxidation (Table 2). Various cyclic olefins such as cyclooctene, cyclohexene, 2-norbornene and α -pinene achieved complete conversion within 4 hours without any by-products in this epoxidation reaction (Entries 1-4). Terminal linear alkenes are generally considered to be inert alkenes with epoxidation. Interestingly, they were also oxidized with good yield and excellent selectivity by prolonging the reaction time (Entries 5-7). For aryl-substituted olefins, although *trans*- β -methylstyrene was oxidized to the corresponding epoxide with outstanding yields (>99%) and selectivity (>99%) within 6 h (Entry 8), the epoxidation of styrene under the same conditions only realized 65% selectivity in 6 h (Entry 9). This was due to the kinetic instability of the styrene oxide, benzaldehyde and phenylpropionaldehyde.³³ In addition, the reactions of disubstituted aromatic olefins were slower (Entries 10-12) and they required 24 h to achieve high conversion due to the steric hindrance effect.³⁴ It is worth noting that the epoxidation rate (>99%) of *trans*-stilbene was much faster than that (85%) of *cis*-isomer as a result of the steric-hindrance effect.³⁵

Table 2 Aerobic epoxidation of olefins catalyzed by DPSNs@Cu-BTC-2^a.

| Entry | Substrate | Product | Time (h) | Con.(%) ^b | Sel.(%) ^b |
|-------|-----------|---------|----------|----------------------|----------------------|
| 1 | | | 4 | >99 | >99 |
| 2 | | | 4 | >99 | >99 |
| 3 | | | 4 | >99 | >99 |
| 4 | | | 4 | >99 | >99 |
| 5 | | | 6 | 89 | >99 |
| 6 | | | 12 | 71 | >99 |
| 7 | | | 24 | 58 | >99 |
| 8 | | | 6 | >99 | >99 |
| 9 | | | 6 | 62 | 65 |
| 10 | | | 24 | 88 | 91 |
| 11 | | | 24 | >99 | >99 |
| 12 | | | 24 | >99 | >99 |

[a] Reaction conditions: 1.0 mmol cyclooctene, 2.0 mol% DPSNs@Cu-BTC-2 based on copper, trimethylacetaldehyde (2.0 mmol), acetonitrile (5.0 mL), 1 atm O₂, 40 °C, 4 h. [b] Nitrobenzene was used as internal standard and determined by GC-MS.

3.3 Recyclability of DPSNs@Cu-BTC

In order to show the advantages of the nanocomposites in the cyclic performance, the epoxidation of cyclooctene was performed using batches of recovered catalyst under previously mentioned conditions. The reaction conditions and catalyst dosage of each cycle remained consistent, and the results after ten cycles are shown in Fig. 8. The DPSNs@Cu-BTC-1 remains 95% conversion and there is no reduction of catalytic activity (Fig. 8a). When the amount of Cu-BTC loaded reaches 17.3 wt.%, the catalytic activity of DPSNs@Cu-BTC-2 begins to decrease after eight cycles, and after ten cycles, the conversion decreases from 99% to 97% (Fig. 8b). The catalytic activity of the DPSNs@Cu-BTC-3 with 33.8 wt.% of the amount loaded begins to decline at the fifth cycle, and the conversion rate is only 92% after ten cycles (Fig. 8c). By comparison, after ten cycles, the cycle reusable performance of the composite catalyst is inversely proportional to the amount of Cu-BTC loaded, i.e., DPSNs@Cu-BTC-1 > DPSNs@Cu-BTC-2 > DPSNs@Cu-BTC-3 > Cu-BTC. XRD and TEM results (Fig. S9) also prove that the morphology and internal structure of the nanocomposite show no obvious change after ten cycles. Significantly, all the DPSNs@Cu-BTC nanocomposites maintain excellent reusability compared with the unsupported Cu-BTC after ten cycles (Fig. 8d).

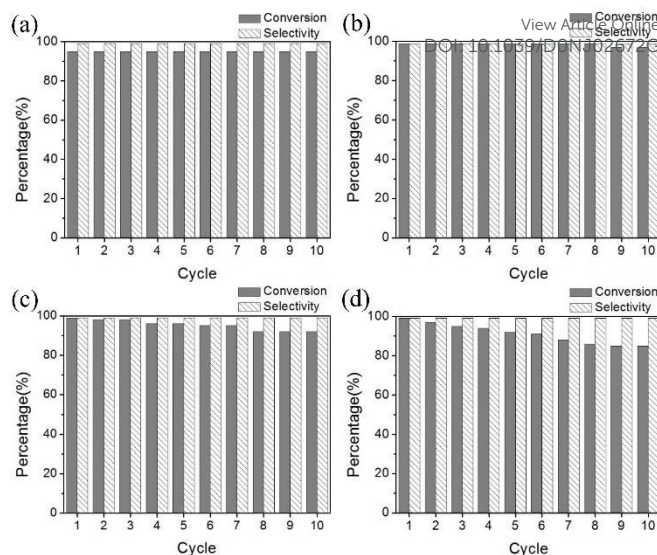


Fig. 8 Recyclability of the DPSNs@Cu-BTC in the epoxidation of cyclooctene: (a) DPSNs@Cu-BTC-1, (b) DPSNs@Cu-BTC-2, (c) DPSNs@Cu-BTC-3, (d) Cu-BTC prepared from Cu₂O NPs.

4. Conclusions

In summary, we successfully prepared a series of DPSNs@Cu-BTC nanocomposites with small-sized Cu-BTC NPs in the center-radial pores of the DPSNs by using DPSNs@Cu₂O as precursor. Moreover, the controlled growth of Cu-BTC in the center-radial pores was realized by adjusting the amount of Cu₂O loaded in the DPSNs. All the DPSNs@Cu-BTC nanocomposites showed good catalytic activity and excellent chemical and reusable stability in the epoxidation of olefins with molecular oxygen as the green oxygen source. Furthermore, the DPSNs@Cu-BTC-2 exhibited the best catalytic activity and reusability after ten cycles. Compared with other fabrication methods, this indirect method for the growth of Cu-BTC in the center-radial pores of DPSNs provides a new idea for the synthesis of nanocomposites and modification of other carriers.

Conflicts of interest

There are no conflicts to declare.

Acknowledgements

This work is financially supported by the Beijing Natural Science Foundation (Grant No. L182020), the National Natural Science Foundation of China (Grant No. 51503016, 51971208, 21501009) and Fundamental Research Funds for the Central Universities (Grant No. FRF-TP-19-013B1).

Notes and references

- G. B. Gardner, D. Venkataraman, J. S. Moore and S. Lee, *Nature*, 1995, **374**, 792–795.

ARTICLE

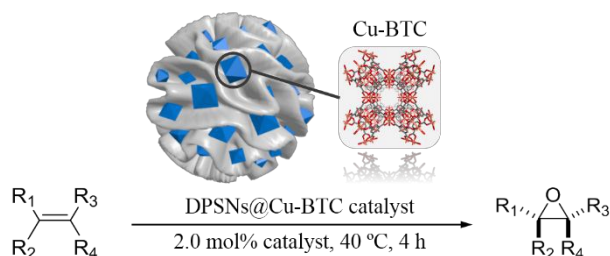
Journal Name

- 1
2
3
4
5
6
7
8
9
10
11
12
13
14
15
16
17
18
19
20
21
22
23
24
25
26
27
28
29
30
31
32
33
34
35
36
37
38
39
40
41
42
43
44
45
46
47
48
49
50
51
52
53
54
55
56
57
58
59
60
- 2 H. Li, M. Eddaoudi, M. O'Keeffe and O. M. Yaghi, *Nature*, 1999, **402**, 276–279.
- 3 A. J. Howarth, Y. Liu, P. Li, Z. Li, T. C. Wang, J. T. Hupp and O. K. Farha, *Nature*, 2016, **1**, 15018–15032.
- 4 P. Garcia-Garcia, M. Mueller and A. Corma, *Chem. Sci.*, 2014, **5**, 2979–3007.
- 5 B. J. Bucior, N. S. Bobbitt, T. Islamoglu, S. Goswami, A. Gopalan, T. Yildirim, O. K. Farha, N. Bagheri and R. Q. Snurr, *Mol. Syst. Des. Eng.*, 2019, **4**, 162–174.
- 6 J. N. Joshi, G. Zhup, J. J. Lee, E. A. Carter, C. W. Jones, R. P. Lively and K. S. Walton, *Langmuir*, 2018, **34**, 8443–8450.
- 7 P. Mahata, S. K. Mondal, D. K. Singha and P. Majee, *Dalton T.*, 2017, **46**, 301–328.
- 8 P. Deria, D. A. Gomez-Gualdrón, I. Hod, R. Q. Snurr, J. T. Hupp and O. K. Farha, *J. Am. Chem. Soc.*, 2016, **138**, 14449–14457.
- 9 M. Heitbaum, F. Glorius and I. Escher, *Angew. Chem. Int. Edit.*, 2006, **45**, 4732–4762.
- 10 L. H. Wee, N. Janssens, S. R. Bajpe, C. E. A. Kirschhock and J. A. Martens, *Catal. Today*, 2011, **171**, 275–280.
- 11 E. Pérez-Mayoral and J. Čejka, *ChemCatChem*, 2011, **3**, 157–159.
- 12 A. Sachse, R. Ameloot, B. Coq, F. Fajula, B. Coasne, D. De Vos and A. Galarneau, *Chem. Commun.*, 2012, **48**, 4749–4751.
- 13 G. Song, Y. Lu, Q. Zhang, F. Wang, X. Ma, X. Huang and Z. Zhang, *RSC Adv.*, 2014, **4**, 30221–30224.
- 14 A. S. Shalygin, A. L. Nuzhdin, G. A. Bukhtiyarova and O. N. Martyanov, *J. Sol-Gel Sci. Technol.*, 2017, **84**, 446–452.
- 15 J. Kou and L. Sun, *ACS Appl. Mater. Interfaces*, 2018, **10**, 12051–12059.
- 16 X. Du and S. Qiao, *Small*, 2015, **11**, 392–413.
- 17 A. Maity and V. Polshettiwar, *ChemSusChem*, 2017, **10**, 3866–3913.
- 18 Y. Wang, X. Du, S. Shi, Z. Liu and H. Lv, *J. Mater. Chem. A*, 2019, **7**, 5111–5152.
- 19 A. Maity, R. Belgamwar and V. Polshettiwar, *Nat. Protoc.*, 2019, **14**, 2177–2204.
- 20 Y. Xing, X. Du, X. Li, H. Huang, J. Li, Y. Wen and X. Zhang, *J. Alloy. Compd.*, 2018, **732**, 70–79.
- 21 H. Chen, Z. Gu, S. Mirza, S. Zhang and J. Zhang, *J. Mater. Chem. A*, 2018, **6**, 7175–7181.
- 22 Z. Gu, D. Zhang, W. Fu, Z. Fu, M. I. Vohra, L. Zhang, C. Wöll and J. Zhang, *Inorg. Chem.*, 2017, **56**, 3526–3531.
- 23 R. Ye, L. Lin, C. Chen, J. Yang, F. Li, X. Zhang, D. Li, Y. Qin, Z. Zhou and Y. Yao, *ACS Catal.*, 2018, **8**, 3382–3394.
- 24 S. K. Bhardwaj, N. Bhardwaj, G. C. Mohanta, P. Kumar, A. L. Sharma, K. Kim and A. Deep, *ACS Appl. Mater. Interfaces*, 2015, **7**, 26124–26130.
- 25 Y. Cao, Y. Xun, H. Hao and G. Zhang, *Mater. Lett.*, 2014, **114**, 88–91.
- 26 Y. Liu, W. Zhang, S. Li, C. Cui, J. Wu, H. Chen and F. Huo, *Chem. Mater.*, 2014, **26**, 1119–1125.
- 27 S. S. Y. Chui, S. M. F. Lo, J. P. H. Charmant, A. G. Orpen and I. D. Williams, *Science*, 1999, **283**, 1148–1150.
- 28 A. R. Abbasi and M. Rizvandi, *Ultrason. Sonochem.*, 2018, **40**, 465–471.
- 29 J. Kim, S. H. Kim, S. T. Yang and W. S. Ahn, *Micropor. Mesopor. Mat.*, 2012, **161**, 48–55.
- 30 D. J. Lee, Q. Li, H. Kim and K. Lee, *Micropor. Mesopor. Mat.*, 2012, **163**, 169–177.
- 31 A. Sahai, N. Goswami, S. D. Kaushik and S. Tripathi, *Appl. Surf. Sci.*, 2016, **390**, 974–983.
- 32 G. Zhan and H. C. Zeng, *Chem. Commun.*, 2016, **52**, 8432–8435.
- 33 J. Zhao, W. Wang, H. Tang, D. Ramella and Y. Luan, *Mol. Catal.*, 2018, **456**, 57–64.
- 34 X. Li, Z. Zhou, Y. Zhao, D. Ramella and Y. Luan, *Appl. Organomet. Chem.*, 2020, **34**, e5445.
- 35 I. Garcia-Bosch, X. Ribas and M. Costas, *Adv. Synth. Catal.*, 2009, **351**, 348–352.

Growth of Cu-BTC MOFs on dendrimer-like porous silica nanospheres for catalytic aerobic epoxidation of olefins

View Article Online
DOI: 10.1039/C9NJ02672G

Zihao Zhou,^a Xiujuan Li,^a Yulin Wang,^a Yi Luan,^{*a} Xiaoyu Li ^{*b} and Xin Du ^{*a}



DPSNs@Cu-BTC was achieved using Dendrimer-like Porous Silica Nanoparticles as support and as an efficient catalyst for olefin epoxidation.